Bull. Mater. Sci., Vol. 34, No. 1, February 2011, pp. 37–43. © Indian Academy of Sciences.

Facile synthesis of poly(*p*-phenylenediamine)/MWCNT nanocomposites and characterization for investigation of structural effects of carbon nanotubes

QUANG LONG PHAM, YUVARAJ HALDORAI, VAN HOA NGUYEN, DIRK TUMA[†] and JAE-JIN SHIM*

School of Display and Chemical Engineering, Yeungnam University, Gyeongsan, Gyeongbuk 712-749, Republic of Korea
[†]BAM Federal Institute of Materials Research and Testing, Richard-Willstätter-Str.11, D-12489 Berlin, Germany

MS received 15 October 2010

Abstract. Poly(*p*-phenylenediamine) (P*p*PD)/carboxylic acid-functionalized multiwalled carbon nanotubes (*c*-MWCNTs) nanocomposites were prepared by chemical oxidative polymerization using potassium persulfate ($K_2S_2O_8$) as an oxidant. Field-emission scanning electron microscopy (FE–SEM) and field-emission transmission electron microscopy (FE–TEM) showed that a tubular layer of P*p*PD was coated on the surface of carbon nanotubes with a thickness of 10–20 nm. FT–IR analysis provided an evidence for the formation of nanocomposites. The thermal stability of nanocomposites was improved by addition of *c*-MWCNTs as confirmed by thermogravimetric analysis (TGA). XRD spectra showed that the crystalline nature of P*p*PD was not affected much by the addition of *c*-MWCNTs. As the content of *c*-MWCNTs was increased, the electrical conductivity of the nanocomposites increased due to the interaction between polymer and nanotubes that enhances electron delocalization.

Keywords. ***p*-Phenylenediamine; multi-walled carbon nanotube; nanocomposite; oxidative polymerization.**

1. Introduction

The discovery of carbon nanotubes (Iijima 1991) (CNTs) has revolutionarily changed the face of the modern society in various fields of study including physics, materials science and chemistry. Scientists and researchers are attracted to the unique shape, size and remarkable physical performance of the nanotubes that possess a very high tensile strength, high thermal stability, high electrical conductivity in a cylindrical shape with a diameter of around 10 nm and length of up to 100 μm. Consequently, nanotubes have found applications in various areas such as electrochemical devices, hydrogen storage, field emission devices, sensor and probes (Baughman *et al* 2002). The incorporation of CNTs into plastic can potentially provide structural materials with dramatically increased modulus and strength. Dalton *et al* (2003) reported a spinning method to make super-tough fibres in which the use of CNTs instantly boosted the mechanical strength of poly(vinyl alcohol) (PVA) fibre hundredfold than that of the bare PVA so that it could reach the strength of spider silk. Additionally, the combination of CNTs with conducting polymers enables the production of nanocomposites with significant improvement in electrical conductivity and thermal stability. Different types of conducting polymers including polyaniline (PANI) (Long *et al* 2004a), polypyrrole (PPy) (Long *et al* 2004b), polythiophene (PTh) (Karim *et al* 2006), and polyacetylene (PA) (Tkachenko *et al* 2009) were proved to interact well with CNTs as proven by the dramatic increase in the conductivity of polymers. Typically, it was reported that the incorporation of 24·8% CNTs increased the room temperature conductivity of PANI by hundred times (Long *et al* 2004a), while 23·1% incorporation enhanced that of PPy by 30 times (Long *et al* 2004b).

Recently, investigations on the derivative of PANI, aromatic diamine polymers, are found to be more attractive since they exhibit more novel multifunctionality than PANI and PPy due to one free amino group per repetitive unit on the polymer chains. Thus, these polymers have shown different characteristics from those widely known conducting PANI and PPy in the application of electrocatalysis, electrochromics, sensors, electrode materials, etc (Li *et al* 2002). *Para*-phenylenediamine (*p*PD), one of the three isomers of phenylenediamine (PD), and its copolymers has been widely studied worldwide. Cataldo (1996) and Li *et al* (2001) reported polymerization of *p*PD by oxidation in aqueous acidic solution with potassium persulfate (KPS) as an oxidant. Poly(*p*PD) (P*p*PD) was believed to have a ladder structure and was somewhat similar to pernigraniline with a specific conductivity of $6{\cdot}3 \times 10^{-6}$ S/cm. In another study,

*Author for correspondence (jjshim@yu.ac.kr)

PANI was copolymerized with different ratios of phenylenediamine isomers by a chemical oxidative polymerization method (Prokeš *et al* 1999). Interestingly, poly(aniline-co-*p*-phenylenediamine) (poly(Ani-co-*p*PD)) had conductivity ranging over more than eleven orders of magnitude with the lower end ascribed to the conductivity of P*p*PD that was negligible. More recently, our group (Haldorai *et al* 2009) synthesized poly(Ani-co-*p*PD)/multi-walled carbon nanotube nanocomposites by *in situ* microemulsion polymerization.

The oxidation mechanism of P*p*PD together with its structures has been reported elsewhere (Ichinohe *et al* 1998; Sestrem *et al* 2009); however, it is unclear about the final result. The synthesis of P*p*PD/MWCNTs nanocomposites has not been studied yet. In the present study, we report the preparation of P*p*PD/*c*-MWCNTs nanocomposites by chemical oxidative polymerization. A number of techniques have been used to analyse the nanocomposites such as FT–IR, FE–TEM, FE–SEM, UV-visible, TGA and XRD.

2. Experimental

2.1 *Materials*

MWCNTs were purchased from Aldrich (>90% pure) with a diameter of 10–20 nm and length of 0·1–10 μm. *p*PD (>97%) from Tokyo Chemical Industry and potassium persulfate (KPS) (>99%) from Aldrich were used as received. Other chemicals were of analytical grade and used without further purification.

2.2 *Oxidation of MWCNTs*

0·5 g of MWCNTs was dispersed in 40 ml of concentrated H_2SO_4 and HNO_3 with a volume ratio of 3:1 using an ultrasonicator for 10 min. The mixture was stirred at 60°C for 24 h and then washed several times with deionized water until the pH reached 7. The resulting acid-functionalized MWCNTs were filtered with 0·2 μm PTFE membrane filter and dried in a vacuum at 70°C for 24 h. This treatment produced carboxylic acid groups (–COOH) on the surfaces of MWCNTs at their defects and shortened the length of the tubes.

2.3 *Preparation of PpPD*

In a typical experiment, 0·015 mol *p*PD was added into a 200 ml flask containing 100 ml of acidic aqueous solution (HCl, 0·1 M). Then, the mixture was pre-cooled and stirred constantly in an ice bath to make a homogenous solution. The oxidant solution was prepared by dissolving 0·015 mol KPS in 50 ml of 0·1 M HCl. After that, the oxidant solution was added dropwise to the monomer solution for 30 min to initiate the polymerization. While stirring, the reaction system was kept for 24 h at room temperature to assure the completion of reaction. Then, it was terminated by pouring acetone into the reaction mixture. The product was washed completely with deionized water to remove impurities such as unreacted monomer, oxidant and HCl. It was then washed with acetone, filtered and dried under a vacuum at 60°C for 24 h.

2.4 *Preparation of PpPD/c-MWCNTs nanocomposites*

Each of 2·5 and 5 wt% *c*-MWCNTs (based on the weight of *p*PD) was dispersed in the solution of 0·015 mol *p*PD in 100 ml of 0·1 M HCl by ultrasonication for 10–15 min. Then, the solution of 0·015 mol KPS in 50 ml of 0·1 M HCl was added drop by drop into the previous solution which was stirred constantly in an ice bath in a period of 30 min to initiate the polymerization. The reaction was kept for 24 h. Acetone was then poured into the reaction mixture to stop polymerization and to precipitate the P*p*PD/*c*-MWCNTs nanocomposite. The purification and drying procedures were the same as those for the synthesis of the bare polymer.

2.5 *Characterization*

The morphology of nanocomposites was determined by FE–SEM (Hitachi, S-4100). Microstructures of the samples were examined by FE–TEM (FEI, Tecnai G2 F20). TGA was performed on a thermal analyser (TA Instruments, SDT Q600) from 40–800°C at a heating rate of 10°C/min under nitrogen atmosphere. For confirmation of crystallinities and structures of *c*-MWCNTs, bare P*p*PD and nanocomposites, X-ray diffraction (XRD) data were collected with a diffractometer (Panalytical, X'Pert Pro MPD) using Cu-Kα radiation sources at an operating voltage of 40 kV. Structural effects of nanocomposites were characterized by FT–IR spectrometer (Bio-Rad, Excalibur FTS 3000) and UV-Visible spectrophotometer (Shimadzu, UV-160A). Room temperature conductivity was measured by the Hall Effect Measurement System (Ecopia, HMS-5000) using the Van der Pauw four-probe method.

3. Results and discussion

3.1 *Acid-functionalized MWCNTs*

Carbon nanotubes functionalized with carboxylic acid groups were confirmed by FT–IR as shown in figure 1. Two bands at around 3350 and 1200 cm^{-1} are assigned to the –OH groups on the surface of pristine MWCNTs (Haldorai *et al* 2009), which might originate from ambient moisture bound to the MWCNTs or be generated during purification of the raw material (Ramanathan *et al* 2005). In the acid-functionalized MWCNTs spectrum, the peak near 1560 cm^{-1} corresponds to the infrared-active phonon mode of the nanotubes (Jeevananda *et al* 2008) and the peaks at

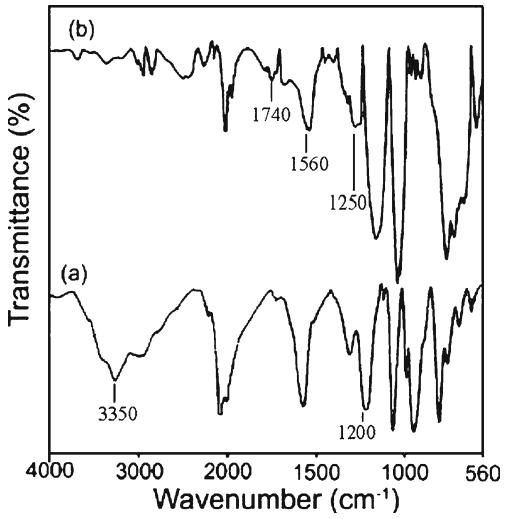

Figure 1. FT–IR spectra of (**a**) pristine MWCNTs and (**b**) *c*-MWCNTs.

1740 and 1250 cm^{-1} apparently correspond to the stretching mode of the carboxylic acid groups (Mawhinney *et al* 2000). These observations are clear indications of –COOH groups on the surface of nanotubes.

The difference in the morphology between pristine MWCNTs and *c*-MWCNTs was confirmed by FE–SEM as shown in figure 2. Pristine MWCNTs which have smooth surfaces appeared as large bundles with lengths in the order of micron and diameters around 10–20 nm. After acid treatment, the *c*-MWCNTs were disentangled and rough, and their lengths were slightly reduced by both the oxidation and ultrasonic treatment.

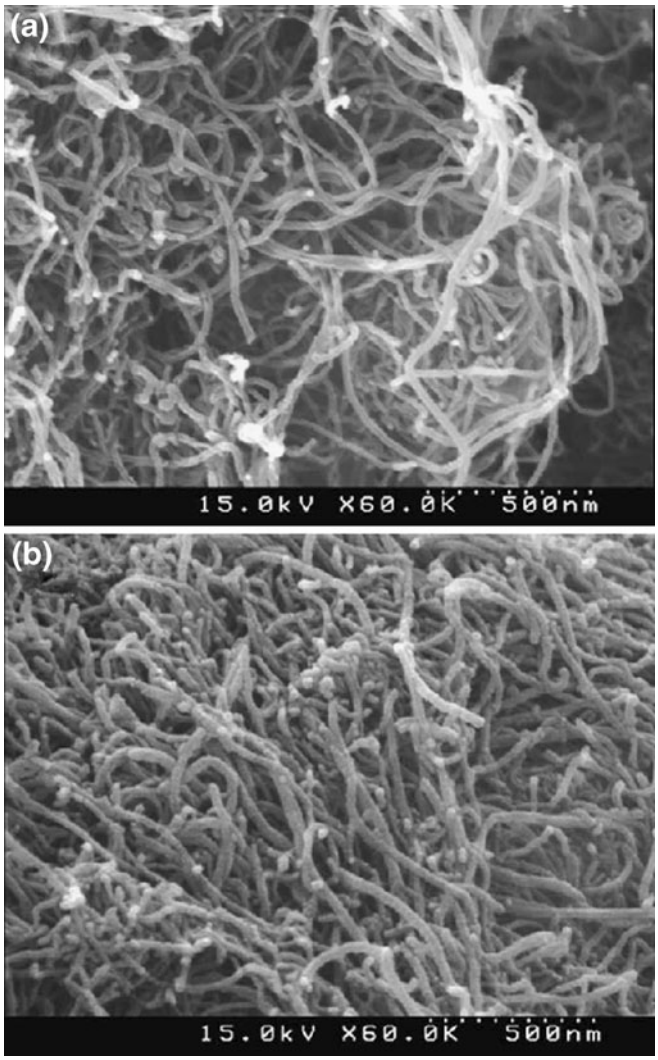

Figure 2. FE–SEM micrographs of (**a**) pristine MWCNTs and (**b**) *c*-MWCNTs.

3.2 *Morphology and structure of bare polymer and nanocomposites*

Scheme 1 interprets the formation of P*p*PD/*c*-MWCNTs nanocomposite. There are three main steps represented by three arrows. The first step is the surface modification of MWCNTs which introduces COOH groups as well as changes the surface morphology of the nanotubes as confirmed by FT–IR and FE–SEM. The second step is the addition of as-prepared *c*-MWCNTs into the acidic solution of *p*PD monomer followed by ultrasonication. Interactions between monomer and the surface of *c*-MWCNTs are depicted in the enlarged picture. Basically, there are two main interactions: one is the H-bonding interaction between the proton in the carboxylic group of *c*-MWCNT and N atoms of monomer, another one is the π–π* interaction between benzenoid ring of *p*PD and the π-system of CNT. Such interactions pledge the strong encapsulation of *c*-MWCNTs by P*p*PD which is formed in polymerization step (the third step). In this last step, polymer is formed by chemical oxidative polymerization of *p*PD with an aid of an oxidant, $K_2S_2O_8$ and the growth of polymer takes place both on the surface of *c*-MWCNTs and in the continuous phase. However, the polymerization reaction is faster on the surface of *c*-MWCNTs in comparison with the continuous phase due to lower activation energy (based on the principle of heterogeneous catalyst).

FE–SEM micrographs of the bare P*p*PD, and nanocomposite with 2·5% *c*-MWCNTs are shown in figure 3. The bare polymer cropped up with non-descriptive shapes, while in the case of P*p*PD/*c*-MWCNTs nanocomposite, a tubular polymer layer was coated on the surface of carbon nanotubes, thus making the diameters of the composites larger than that of *c*-MWCNTs as reflected in figure 2b. In order to confirm the coating of polymer on the surface of carbon nanotubes, FE–TEM image of the composite with 2·5% *c*-MWCNTs

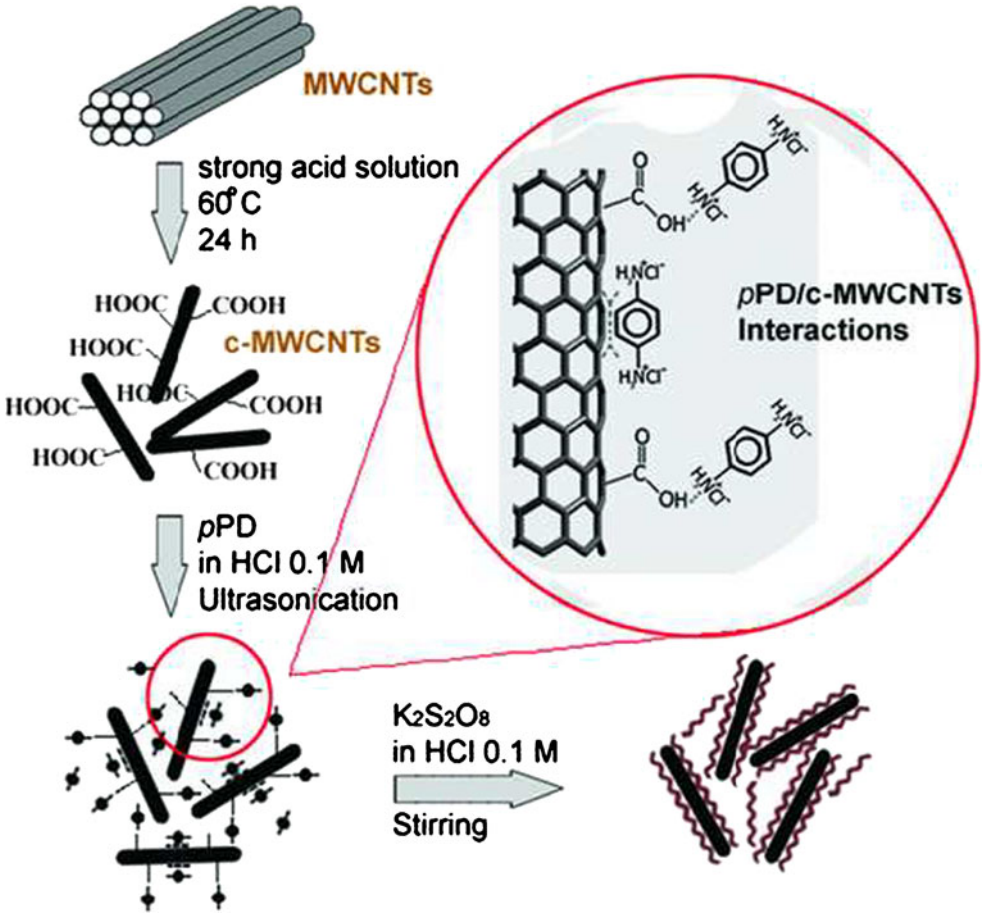

Scheme 1. A schematic illustration of the formation of P*p*PD/*c*-MWCNTs nanocomposite.

was taken. A core-shell structure was clearly observed in its expanded view (figure 3d). The core is a nanotube with a diameter of 10–20 nm, whereas the shell is made up of the polymer with a thickness of 10–20 nm. As shown in figure 3c, the polymer layer was uniformly grown on the surface of nanotubes to form the tubular nanocomposite. Formation of the polymer coating on the surface of CNTs can be explained by the absorption of *p*PD monomer onto the surface of CNTs during polymerization (Jeevananda *et al* 2008).

3.3 *UV-Vis spectra*

UV-Visible spectra of the bare polymer and nanocomposite with 5% *c*-MWCNTs in N-methyl-2-pyrrolidone (NMP) are shown in figure 4. Both samples showed similar curve patterns. A shoulder band at around 270 nm and a strong absorption band at 305 nm are assigned to the π–π^* transition of the benzenoid rings of the polymer (Haldorai *et al* 2009). The broad band centred at ~430 nm is attributable to the polaron–π transition on P*p*PD chain, typically, in some places it resembles the emeraldine salt structure of polyaniline (PANI–ES) (Wu *et al* 2005; Sestrem *et al* 2009). There is a slight difference in the spectra of P*p*PD/*c*-MWCNT composite from those of the bare polymer. By comparing the relative heights for the peaks at 305 nm and 430 nm, we can see that the band at 430 nm in the nanocomposite showed a higher absorption than that in the bare polymer. This result suggests that there is an interaction between the quinoid rings of P*p*PD and *c*-MWCNTs that enhances the formation of the polaron–π transition of the polymer chain.

3.4 *FT–IR spectra*

FT–IR spectra of the bare polymer and nanocomposites with 2·5% and 5% *c*-MWCNTs are shown in figure 5. A broad peak centred at around 3450 cm^{-1} originates from the N–H stretching vibration of secondary amine group in the polymer chain. The peaks at 1602 and 1493 cm^{-1} are assigned to the C=N and C=C stretching vibrations in quinoid and benzenoid rings, respectively (Li *et al* 2002). The indication of the imine C–N absorption showed a small peak at about 1300 cm^{-1}, and the peak at 830 cm^{-1} can be ascribed to the out-of-plane bending vibration of benzene ring

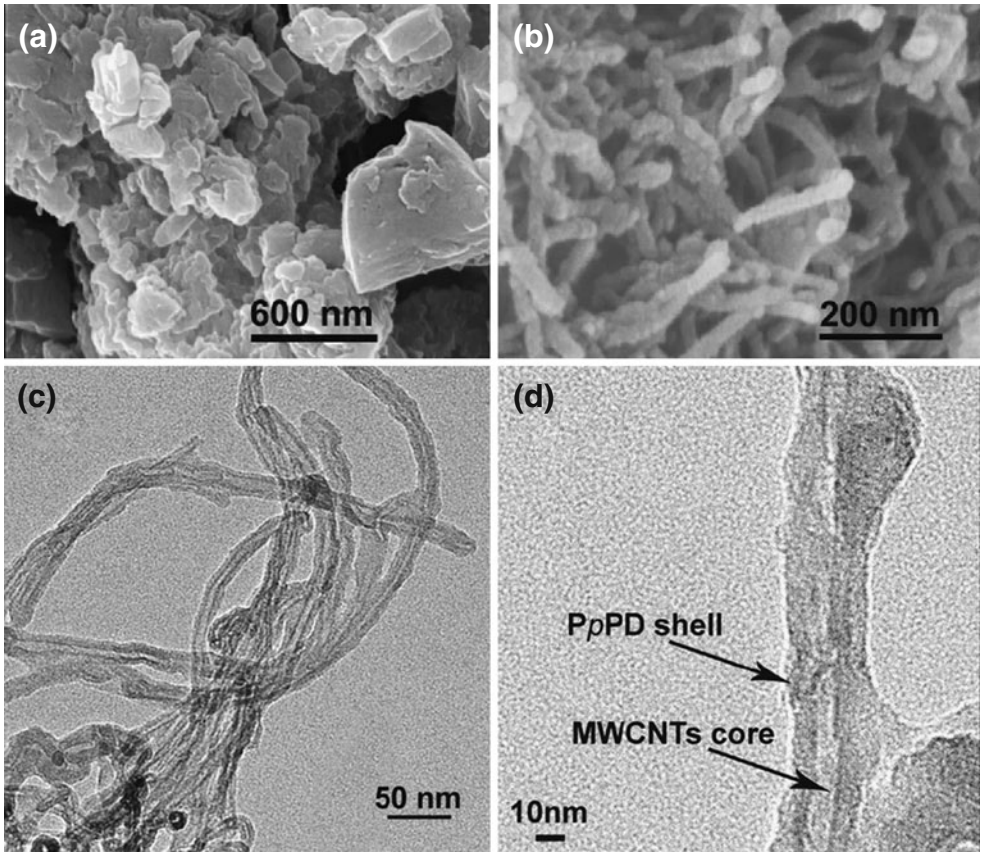

Figure 3. FE–SEM micrographs of (**a**) bare polymer and (**b**) nanocomposite with 2·5% *c*-MWCNTs. FE–TEM micrographs of (**c**) nanocomposite with 2·5% *c*-MWCNTs and (**d**) its expanded view.

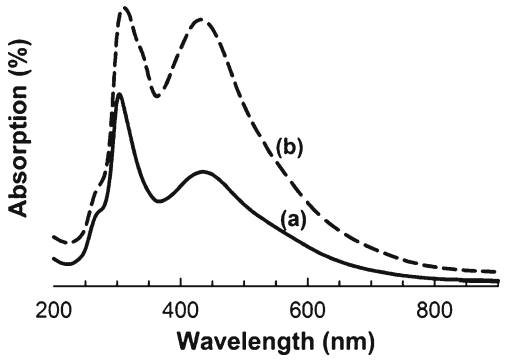

Figure 4. UV-visible spectra of (**a**) bare polymer and (**b**) nanocomposite with 5% *c*-MWCNTs.

(Haldorai *et al* 2009). The strong band at around 1132 cm^{-1} was supposed to be "electron-like band" which is considered to be a measure of delocalization (Cataldo 1996). The change in the intensity ratio of the quinoid and benzenoid peaks was observed between the bare polymer and composites. This result may be due to the discrepancy in the polymer structures of those polymerized in the continuous phase and those growing on the surface of carbon nanotubes. In the latter case, less benzenoid units were formed, as evidenced by the reduction in the relative strength of IR signals at 1602 cm^{-1} and 1493 cm^{-1}. Similar results were observed by others also (Cataldo 1996).

3.5 *XRD spectra*

In order to confirm the influence of carbon nanotubes on the crystal structure of P*p*PD, XRD spectra of *c*-MWCNTs, bare polymer, and nanocomposites of 2·5% *c*-MWCNTs and 5% *c*-MWCNTs are shown in figure 6. Diffraction pattern of *c*-MWCNTs is characterized by a strong peak at $2\theta = 25{\cdot}9°$ which is ascribed to the graphite-like structure (Wu *et al* 2005). In the spectrum of bare polymer, there are several peaks that represent the crystalline nature of the polymer: a low-intensity broad peak at 14°, a high-intensity sharp peak at around 16·3°, a broad peak at 18·3°, and a sharp peak at 19·1°. A large, broad bump of a low-intensity peak centred at 25° is attributed to the amorphous portion of P*p*PD synthesized by oxidative polymerization that fairly correlates with XRD spectrum of P*p*PD reported by Li *et al* (2001).

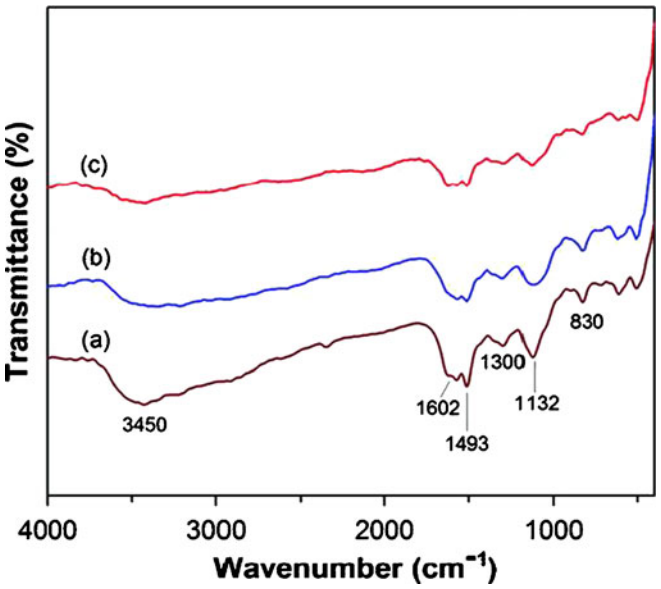

Figure 5. FT–IR spectra of (**a**) bare polymer, (**b**) nanocomposite with 2·5% *c*-MWCNTs and (**c**) nanocomposite with 5% *c*-MWCNTs.

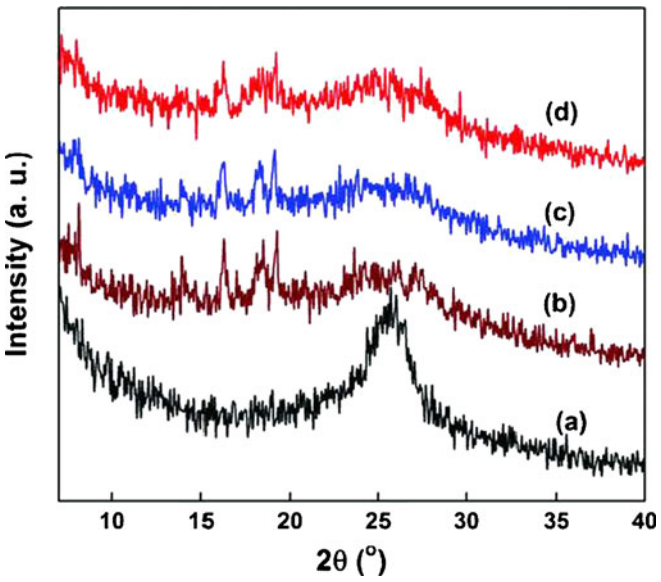

Figure 6. XRD patterns of (**a**) *c*-MWCNTs, (**b**) bare polymer, (**c**) nanocomposite with 2·5% *c*-MWCNTs and (**d**) nanocomposite with 5% *c*-MWCNTs.

The addition of *c*-MWCNTs into the polymer matrix did not cause a discernible change in the lattice structure of P*p*PD as can be seen in figure 6. There was only a small reduction in the sharpness of the crystalline peaks, as CNTs were present in the polymer matrix and it slightly changed the crystal nature of the bare polymer.

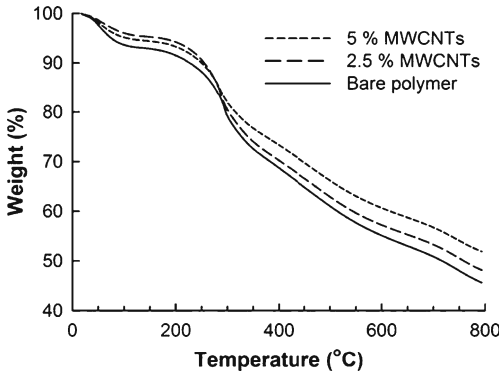

Figure 7. TGA curves of the bare polymer and nanocomposites in nitrogen.

3.6 *Thermal stability*

Thermal stability of bare polymer and nanocomposites is shown in figure 7. The shapes of those curves are similar to each other, as they reflect two main stages of weight loss. The first weight loss step between 50 and 140°C is due to the loss of moisture, vaporization of solvent, and residual HCl absorbed by the polymer. The second step starting from 170°C is attributed to the decomposition of polymer. We can see that the bare polymer decomposed at a higher rate than polymer in the nanocomposites. The extent of decomposition declined as more *c*-MWCNTs were added, as evidenced by less weight loss in the 5 wt% sample in comparison with the 2·5 wt% one. This suggests that the addition of *c*-MWCNTs improved the thermal stability of polymer that was correlated well with other studies (Jeevananda *et al* 2008; Haldorai *et al* 2009).

3.7 *Conductivity*

Conductivity of bare polymer and nanocomposites was measured using a four-point probe method at room temperature. The results are given in table 1. According to the previous studies (Cataldo 1996; Prokeš *et al* 1999; Lakard *et al* 2003), conductivity of neat P*p*PD is nearly negligible, so it is not surprising that we could not get any data for this sample because its conductivity was below the lower limitation of the instrument. This indicates that the bare polymer is almost

Table 1. Conductivities of bare polymer and nanocomposites measured at 300K. (Data shown here represent the mean measurement values of at least 3 different positions on the surfaces of the samples).

Samples	Conductivity (S/cm)
Bare P*p*PD	N/A
Nanocomposites with 2·5% *c*-MWCNTs	$\sim 2 \times 10^{-6}$
Nanocomposites with 5% *c*-MWCNTs	$\sim 8 \times 10^{-3}$

an insulator. In contrast, the nanocomposites showed better conductivity and the conductivity increased with increasing nanotube content. Interestingly, with increase in *c*-MWCNTs content from 2·5% to 5%, the conductivity of the nanocomposite increased by three orders of magnitude. This improvement is due to the π–π^* interaction between the surfaces of *c*-MWCNTs and the quinoid ring of P*p*PD (Haldorai *et al* 2009), which effectively improved the degree of electron delocalization between the two components, as confirmed by FT–IR and UV–Vis spectra.

4. Conclusions

We have successfully synthesized nanocomposites consisting of P*p*PD and acid-functionalized MWCNTs using chemical oxidative polymerization. Morphological studies by FE–SEM and FE–TEM revealed the core-shell structure of nanocomposite with nanotube as the core and a coating layer of P*p*PD as the shell with a thickness of 10–20 nm. The addition of *c*-MWCNTs into the polymer improved both thermal stability and electrical conductivity, but did not influence the crystalline nature of the bare polymer to any great extent, as confirmed by XRD. The bare polymer was almost an insulator; however, the nanocomposites showed better conductivity, ranging from 2×10^{-6} to 8×10^{-3} S/cm. The improved conductivity can apparently be understood from the interaction between *c*-MWCNTs and the polymer chains.

Acknowledgement

This work was supported by the Korea Research Foundation Grant funded by the Korean Government (KRF-2010-0016445).

References

Baughman R H, Zakhidov A A and de Heer W A D 2002 *Science* **297** 787

Cataldo F 1996 *Eur. Polym. J.* **32** 43

Dalton A B, Collins S, Muñoz E, Razal J M, Von Howard E, Ferraris J P, Coleman J N, Kim B G and Baughman R H 2003 *Nature* **423** 703

Haldorai Y, Lyoo W S and Shim J J 2009 *Colloid Polym. Sci.* **287** 1273

Ichinohe D, Saitoh N and Kise H 1998 *Macromol. Chem. Phys.* **199** 1241

Iijima S 1991 *Nature* **354** 56

Jeevananda T, Siddaramaiah, Kim N H, Heo S B and Lee J H 2008 *Polym. Adv. Technol.* **19** 1754

Karim M R, Lee C J and Lee M S 2006 *J. Polym. Sci. Part A: Polym. Chem.* **44** 5283

Lakard B, Herlem G, Lakard S and Fahys B 2003 *J. Mol. Struct. (Theochem.)* **638** 177

Li X G, Huang M R, Chen R F, Jin Y and Yang Y L 2001 *J. Appl. Polym. Sci.* **81** 3107

Li X G, Huang M R and Duan W 2002 *Chem. Rev.* **102** 2925

Long Y Z, Chen Z J, Zhang X T, Zhang J and Liu Z F 2004a *Appl. Phys. Lett.* **85** 1796

Long Y Z, Chen Z J, Zhang X T, Zhang J and Liu Z F 2004b *J. Phys. D: Appl. Phys.* **37** 1965

Mawhinney D B, Naumenko V, Kuznetsova A, Yates Jr. J T, Liu J and Smalley R E 2000 *J. Am. Chem. Soc.* **122** 2383

Prokeš J, Stejskal J, Křivka I and Tobolková E 1999 *Synth. Met.* **102** 1205

Ramanathan T, Fisher F T, Ruoff R S and Brinson L C 2005 *Chem. Mater.* **17** 1290

Sestrem R H, Ferreira D C, Landers R, Temperini M L A and do Nascimento G M D 2009 *Polymer* **50** 6043

Tkachenko L I, Efimov O N, Anoshkin I V, Kulova T L, Roshchupkina O S, Shul'ga Yu M and Petrova N K 2009 *Russ. J. Electrochem.* **45** 296

Wu T M, Lin Y W and Liao C S 2005 *Carbon* **43** 734